2635

Geophysical Research Letters

RESEARCH LETTER
10.1029/2018GL079714

Key Points:
- CMIP5 models project an increase in California wintertime extreme precipitation
- The bulk of the increase is due to moistening of the warmer atmosphere
- The responses are larger in models that better simulate the El Niño-California precipitation teleconnection

Supporting Information:
- Supporting Information S1

Correspondence to:
Robert J. Allen,
rjallen@ucr.edu

Citation:
Zecca, K., Allen, R. J., & Anderson, R. G. (2018). Importance of the El Niño teleconnection to the 21st century California wintertime extreme precipitation increase. *Geophysical Research Letters*, *45*. https://doi.org/10.1029/2018GL079714

Received 23 JUL 2018
Accepted 26 SEP 2018
Accepted article online 1 OCT 2018

Importance of the El Niño Teleconnection to the 21st Century California Wintertime Extreme Precipitation Increase

Katherina Zecca[1], Robert J. Allen[1], and Ray G. Anderson[2]

[1]Department of Earth Sciences, University of California, Riverside, CA, USA, [2]US Salinity Laboratory, George E. Brown, Jr., Salinity Laboratory, USDA-Agricultural Research Service, Riverside, CA, USA

Abstract Under continued climate warming, California (CA) hydrological projections, particularly precipitation, exhibit significant uncertainty. Recent analyses, however, have indicated a tendency for increased CA precipitation through the 21st century, particularly during December-January-February (DJF). Here we show that this increase is due entirely to an increase in extreme (>90th percentile) daily precipitation. This response is consistent with enhanced horizontal vapor transport off the CA coast, most of which is caused by thermodynamical effects due to increases in atmospheric moisture. Furthermore, observations over the late twentieth century show that CA DJF extreme precipitation is associated with an El Niño-like sea surface temperature anomaly pattern. Models that better simulate the observed El Niño teleconnection with CA DJF precipitation also better reproduce the El Niño-like sea surface temperature anomaly pattern associated with extreme precipitation, including the associated thermodynamical and dynamical atmospheric responses. In turn, these models simulate a significantly larger increase in extreme precipitation under warming.

Plain Language Summary In a warmer world, future California hydrological changes remain uncertain. Here we analyze state-of-the-art model simulations and find an increase in California precipitation during the winter. Nearly all of this increase is due to an increase in extreme precipitation, associated with moistening of the warmer atmosphere. Moreover, models that better simulate the El Niño-California precipitation teleconnection yield larger increases in extreme precipitation. This is related to better simulation of the dynamical and thermodynamical atmospheric responses associated with extreme California precipitation.

1. Introduction

Significant uncertainty in 21st century California (CA) precipitation projections exist, with the newer Coupled Model Intercomparison Project version 5 (CMIP5; Taylor et al., 2012) models tending to yield a more consistent increase, particularly in central and Southern CA during December-January-February (DJF; Neelin et al., 2013). Chang et al. (2015) associated this with an eastward shift of the east Pacific upper level winds and a corresponding extension of the storm track toward CA. Similarly, Allen and Luptowitz (2017) linked the increase in CA DJF precipitation to changes in the mean circulation that resembled an El Niño teleconnection. Models that better simulate the observed El Niño-CA precipitation teleconnection yielded larger and more consistent increases in 21st century CA DJF precipitation. This, in turn, was associated with muted drought risk, implying that future CA drought projections are dependent on model fidelity of the El Niño teleconnection.

To better understand uncertainties in the seasonal CA precipitation response, some studies have investigated the change in the frequency and intensity of daily wintertime precipitation. Warner et al. (2015) and Payne and Magnusdottir (2015) found an increase in extreme precipitation events (i.e., atmospheric rivers), and attributed this to an increase in horizontal vapor transport along the West Coast. Similar increases in extreme precipitation and atmospheric rivers in a warmer world have also been noted by others (Dettinger, 2011; Hagos et al., 2016; Lavers et al., 2015). Swain et al. (2018) found an increase in extreme dry-to-wet CA precipitation events, implying an increase in CA precipitation volatility through the 21st century, as well as increases in extreme wet seasons and 40-day accumulations. Similarly, Polade et al. (2017) argued that dynamical mechanisms, including southeastward extension of the Aleutian low from the northwest, as well as thermodynamic

moistening of the warming atmosphere, conspire to yield more horizontal vapor transport and extreme CA precipitation.

Here we expand upon these prior studies, focusing on CA daily extreme precipitation responses under a 21st century high emission scenario and the importance of the El Niño teleconnection. We show that CA DJF extreme precipitation is related to warming of the central/eastern tropical Pacific sea surface temperatures (SSTs). Models that better simulate the El Niño-CA precipitation teleconnection also better simulate this relationship and, in turn, yield larger increases in future CA DJF extreme precipitation. Thus, projections of future CA extreme precipitation depend on model fidelity of the El Niño-CA precipitation teleconnection. This paper is organized as follows: Section 2 lists our methods and data sets, and section 3 discusses results. Conclusions are presented in section 4.

2. Methods

Relevant daily data for the historical and Representative Concentration Pathway 8.5 (RCP8.5) simulation exists for 29 CMIP5 models, with a total of 44 realizations (supporting information Table S1). Daily data include precipitation, sea level pressure, geopotential heights, horizontal winds, and specific humidity. Also included is the 21st century detrended DJF correlation between Niño 3.4 SSTs and CA precipitation, which is used to stratify the models according to their ability to simulate the El Niño teleconnection. Observations from 1948/1949 to 2014/2015 yield a significant correlation between Niño 3.4 SSTs (5°S–5°N; 190°–240°E) and CA DJF precipitation of ∼0.3–0.4. Not all El Niño winters are wetter than normal, nor are all La Niña winters drier than normal. Some evidence also suggests that the teleconnection may not be stationary through time (Coats et al., 2013; Deser et al., 2017; Pavia, 2017), and a new analysis argues that a stronger teleconnection exists based on late-summer SSTs close to New Zealand (Mamalakis et al., 2018). Nonetheless, the El Niño teleconnection represents a reasonably strong pathway by which CA precipitation variations occur.

As defined in Allen and Luptowitz (2017), "models with a 21st century detrended CA DJF precipitation versus Niño 3.4 SST correlation of at least 0.30 are referred to as CMIP5 HIGH−r; models that yield a corresponding correlation less than 0.20 referred to as CMIP5 LOW−r. We also define an alternative CMIP5 HIGH−r model subset that satisfies the following criteria: (1) late twentieth and twenty-first century correlations between DJF CA precipitation and Niño 3.4 SSTs are significant at the 90% confidence level; (2) late 20th century DJF CA precipitation versus Niño 3.4 SST regression coefficient falls within 1-sigma of the observed range; and (3) late 20th century DJF CA precipitation climatologies fall within 1-sigma of the observed range." These models are the same as those in Allen and Luptowitz (2017), except that a smaller subset is used here due to limited availability of the required daily data. CMIP5 HIGH−r contains 12 models and 20 realizations (6 models and 13 realizations using the alternative definition); CMIP5 LOW−r contains 7 models and 11 realizations.

Daily atmospheric data, including sea level pressure, geopotential heights, winds, and specific humidity, come from the National Center for Environmental Prediction/National Center for Atmospheric Research Reanalysis (Kalnay et al., 1996). Daily SST data come from the National Oceanic and Atmospheric Administration's 0.25 × 0.25° resolution Advanced Very High Resolution Radiometer-only Optimum Interpolation SST data set, which spans 1982 to present (Banzon et al., 2016; Reynolds et al., 2007). Daily precipitation observations come from the Climate Prediction Center Global Unified Gauge-Based Analysis of Daily Precipitation, which spans 1979 to present and has a spatial resolution of 0.5 × 0.5° (Chen et al., 2008; Xie et al., 2007).

Unless otherwise noted, all reanalysis/observation-based results span the Advanced Very High Resolution Radiometer time period, 1982–2016. Furthermore, all dynamic and thermodynamic responses/climatologies are based on DJF days with CA extreme precipitation, defined as daily precipitation exceeding the 90th percentile over the late twentieth century. The 90th percentile is estimated by sorting the daily wintertime CA precipitation values from low to high and taking the 0.90•*N*th value, where N is the number of wintertime days. CA is defined by three boxes: Southern CA (32.0°–34.9°N; 239.4°–245.6°E), central CA (34.9°–38.6°N; 236.9°–243.1°E), and Northern CA (38.8°–42.4°N; 235.6°–240.6°E). Unless otherwise noted, figures and analyses are based on the entire state. All data are regridded to a uniform 1.25 × 0.9° spatial grid. We address the *drizzle problem* (Wehner et al., 2010) in climate models by setting all daily precipitation < 1 mm/day to 0. Model responses are estimated as the difference between two 50-year time periods, 2050–2099 minus 1950–1999. CMIP5 twentieth century climatologies are also based on the 1950–1999 historical simulation.

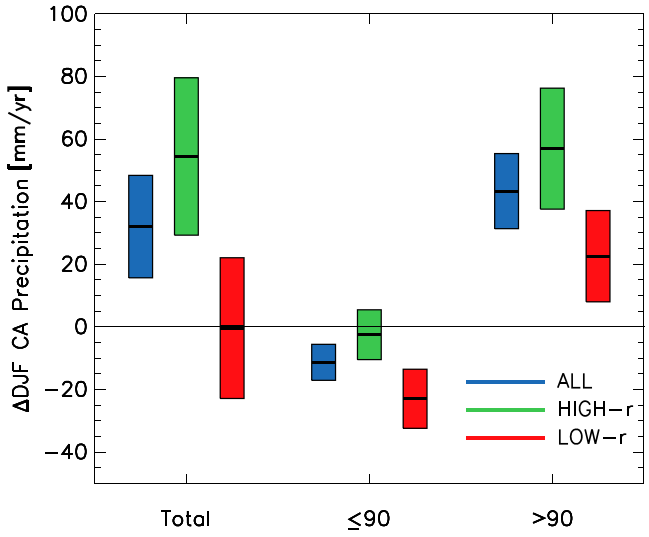

Figure 1. Wintertime California precipitation response in Coupled Model Intercomparison Project version 5 models. The 2050–2099 relative to the 1950-1999 ensemble mean change (center of bar) in December-January-February (DJF) California precipitation for total precipitation, nonextreme (<90th percentile), and extreme (≥90th percentile) precipitation. Length of bars represents uncertainty of the mean change, estimated as $2\sigma/\sqrt{n}$, where n is the number of model realizations and σ is the standard deviation of the responses. Results are shown for all CMIP5 models (ALL; blue); the model subset that yields a detrended DJF Niño 3.4 sea surface temperature versus California precipitation correlation of at least 0.30 (HIGH−r; green); and the model subset that yields a corresponding correlation less than 0.20 (LOW−r; red). Units are millimeters per year.

Integrated vapor transport (IVT) is calculated as

$$\frac{1}{g}\int_{p_s}^{p_t} q\mathbf{V}\,dp, \tag{1}$$

where $\mathbf{V}$ is the horizontal wind velocity (m/s), q is the specific humidity (kg/kg), p_s is 1,000 hPa, p_t is 250 hPa, dp is the difference in pressure between layers, and g is the acceleration of gravity (m/s^2). Pressure levels used to calculate IVT include 1,000, 850, 700, 500, and 250 hPa.

We also approximate the change in IVT (Payne & Magnusdottir, 2015; Seager et al., 2010; Seager et al., 2014; Trenberth & Guillemot, 1995) as

$$\delta IVT \approx \frac{1}{g}\int_{p_s}^{p_t} \delta\bar{q}\overline{\mathbf{V}} + \bar{q}\delta\overline{\mathbf{V}} + \delta(\overline{\mathbf{V}'q'})\,dp, \tag{2}$$

where $\delta(\bullet) = (\bullet)_{\mathrm{RCP85}} - (\bullet)_{\mathrm{historical}}$; overbars represent averages over extreme precipitation days, and primes denote daily anomalies. The first term of equation (2) represents the thermodynamic response; the second term represents the dynamic response; and the third term represents the transient eddy response of IVT to warming.

Precipitable water (PW) is calculated as

$$\frac{1}{g\rho_w}\int_{p_s}^{p_t} q\,dp, \tag{3}$$

where ρ_w is 1,000 kg/m^3. Pressure levels used to calculate PW include 1,000, 850, 700, 500, and 250 hPa.

3. Results

Figure 1 shows the ensemble mean wintertime CA precipitation response in CMIP5 models, broken down by total, nonextreme (≤90th percentile) and extreme (>90th percentile) precipitation. The entire CMIP5 archive (CMIP5 ALL) yields a CA DJF total precipitation increase of 32 mm/year, which represents a 10% increase. All of this increase, however, comes from an increase in extreme precipitation. Nonextreme precipitation decreases by −11 mm/year, or −5%, whereas extreme precipitation increases by 43 mm/year (47% increase). Models therefore project a wetter winter, and nearly all of this increase in precipitation is from extreme events.

As found by Allen and Luptowitz (2017), models that better simulate the El Niño teleconnection with CA DJF precipitation yield a stronger response. CMIP5 HIGH−r yields a CA DJF total precipitation increase of 54 mm/year (17% increase). Nonextreme precipitation decreases by −3 mm/year, whereas extreme precipitation increases by 57 mm/year (59% increase). In contrast, CMIP5 LOW−r yields a negligible change in CA DJF total precipitation at −1 mm/year. This is decomposed into a −23-mm/year (−11%) decrease in nonextreme precipitation and a 22-mm/year (28%) increase in extreme precipitation. Furthermore, the alternative definition of HIGH−r models (section 2) yields similar results, including a nonextreme precipitation decrease of −4 mm/year and an increase in extreme precipitation of 61 mm/year. Thus, models that better simulate the El Niño-CA precipitation teleconnection yield significantly more extreme precipitation. Similar conclusions are obtained for each CA subregion (supporting information Figure S1), with the largest (smallest) increase in total and extreme DJF precipitation in Northern (Southern) CA.

Figure 2 shows late twentieth century spatial climatologies associated with CA DJF extreme precipitation. Observations show that extreme precipitation is associated with an El Niño-like SST anomaly pattern, with warming of the tropical Pacific. CMIP5 HIGH−r also shows a similar relationship, whereas CMIP5 LOW−r yields much weaker tropical Pacific SST warming. Thus, CA DJF extreme precipitation is associated with anomalous warmth of the tropical Pacific SSTs, and CMIP5 HIGH−r models better simulate this relationship. Similar results are obtained for each of the three subregions of CA, with the strongest (weakest) relationship for Southern (Northern) CA (supporting information Figures S2–S4).

Furthermore, observations (National Center for Environmental Prediction/National Center for Atmospheric Research Reanalysis) show that CA DJF daily extreme precipitation is associated with an increase in PW and

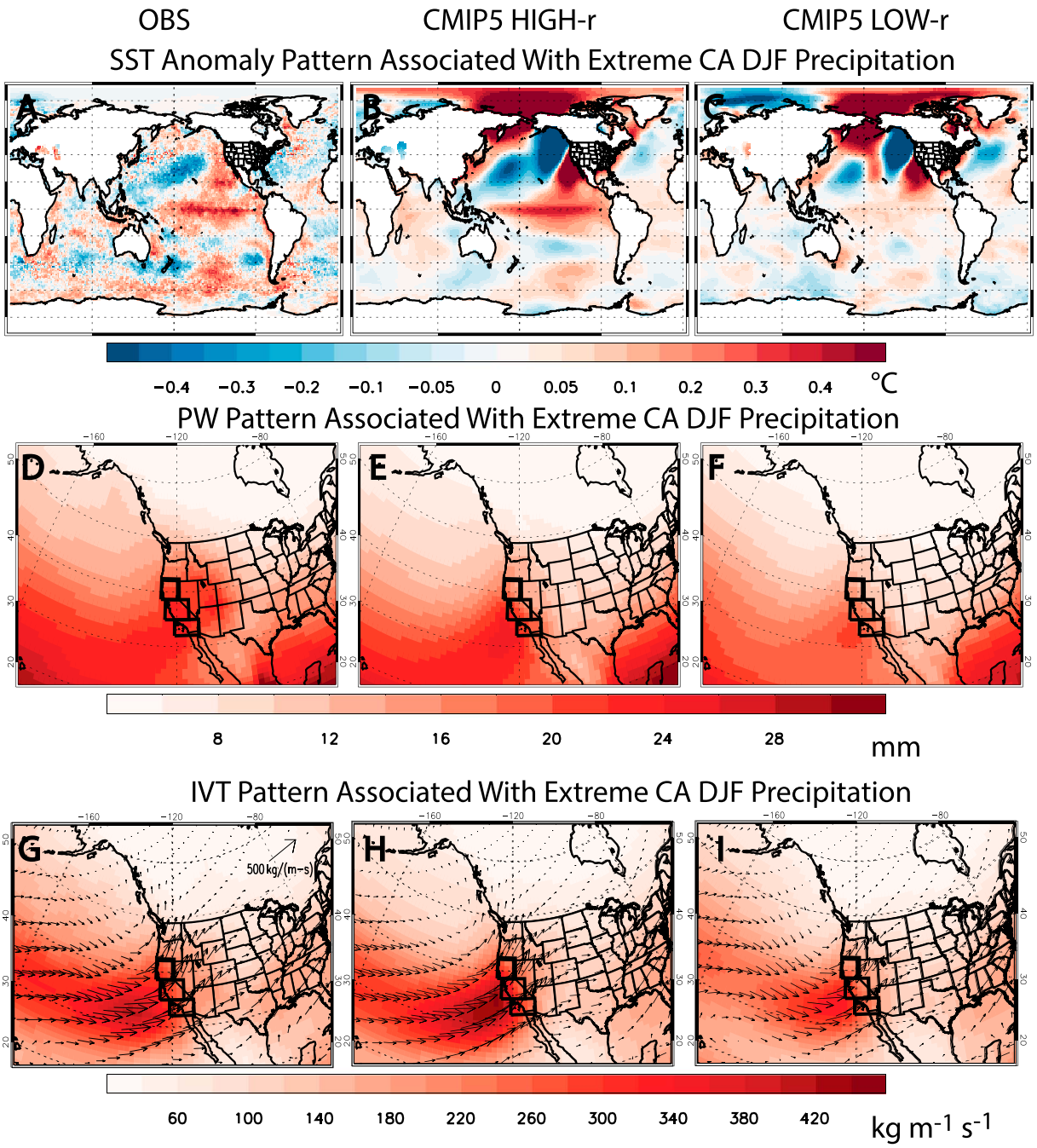

Figure 2. Late twentieth century spatial patterns associated with California wintertime extreme precipitation. (a–c) SST anomalies, (d–f) PW, and (g–i) IVT. Left column shows observations, including NOAA's AVHRR-only Optimum Interpolation SST data and NCEP/NCAR Reanalysis PW and IVT. Middle column shows the CMIP5 ensemble mean for the model subset that yields a detrended DJF Niño 3.4 SST versus California precipitation correlation of at least 0.30 (HIGH−r). Right column shows the model subset that yields a corresponding correlation less than 0.20 (LOW−r). Also included are the three regions comprising California. Observations span 1982–2014, due to AVHRR data limitations. Model results span 1950–1999. Observed daily precipitation data come from NOAA's CPC Global Unified Gauge-Based Analysis. Units are degrees Celsius for SST; millimeters for PW; and kilograms per meter per second for IVT. SST = sea surface temperature; PW = precipitable water; IVT = integrated vapor transport; NOAA = National Oceanic and Atmospheric Administration; AVHRR = Advanced Very High Resolution Radiometer; NCEP/NCAR = National Center for Environmental Prediction/National Center for Atmospheric Research; CMIP5 = Coupled Model Intercomparison Project version 5; DJF = December-January-February; CPC = Climate Prediction Center.

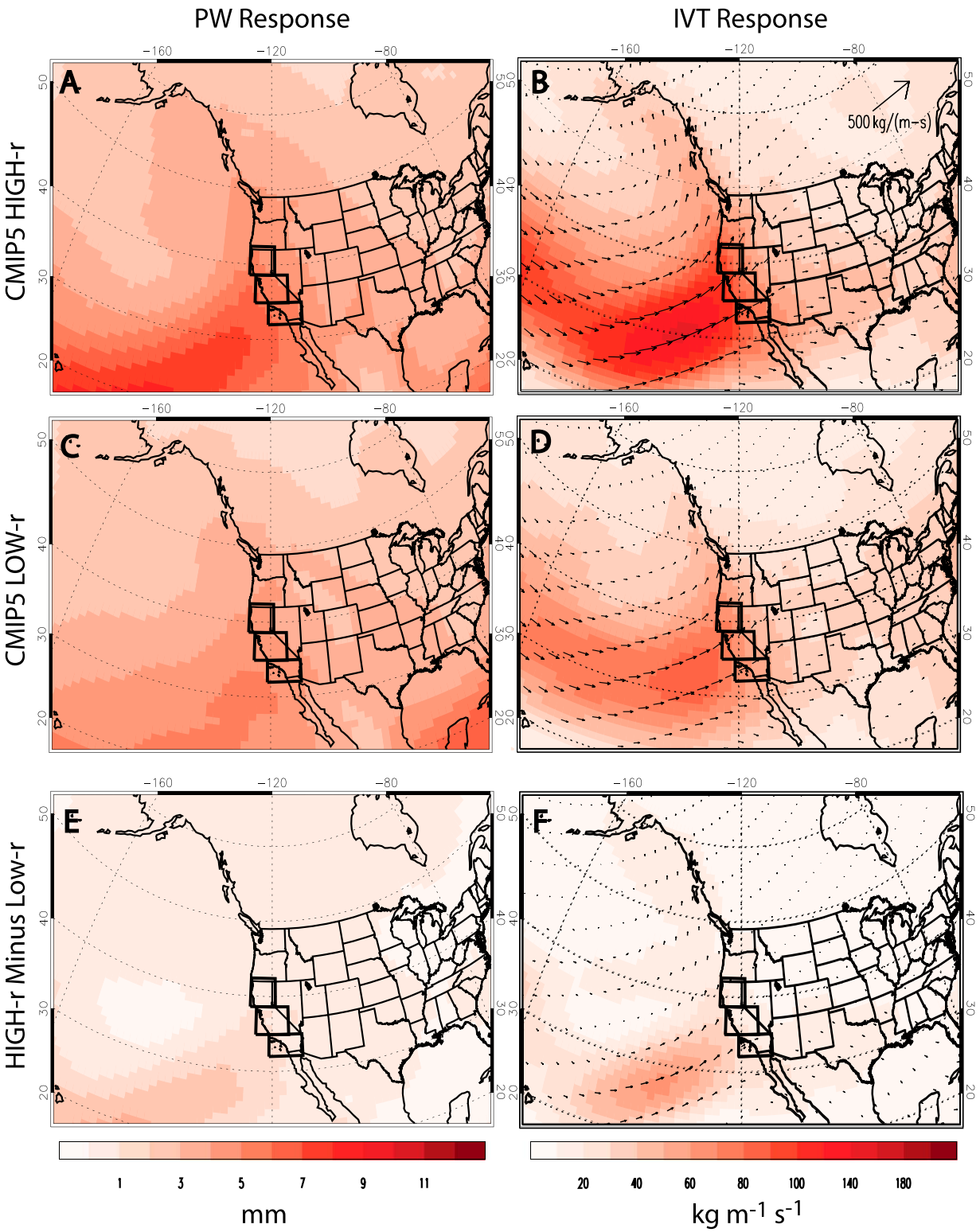

Figure 3. Precipitable water and integrated vapor transport response associated with California wintertime extreme precipitation. Ensemble mean change (2050–2099 minus 1950–1999) in DJF (a, c, e) PW and (b, d, f) IVT associated with extreme precipitation events. Top row shows the CMIP5 ensemble mean for the model subset that yields a detrended DJF Niño 3.4 sea surface temperature versus California precipitation correlation of at least 0.30 (HIGH−r); middle row shows the model subset that yields a corresponding correlation less than 0.20 (LOW−r), and bottom row shows the HIGH−r minus LOW−r difference. Also included are the three regions comprising California. Units are millimeters for PW and kilograms per meter per second for IVT. DJF = December-January-February; PW = precipitable water; IVT = integrated vapor transport; CMIP5 = Coupled Model Intercomparison Project version 5.

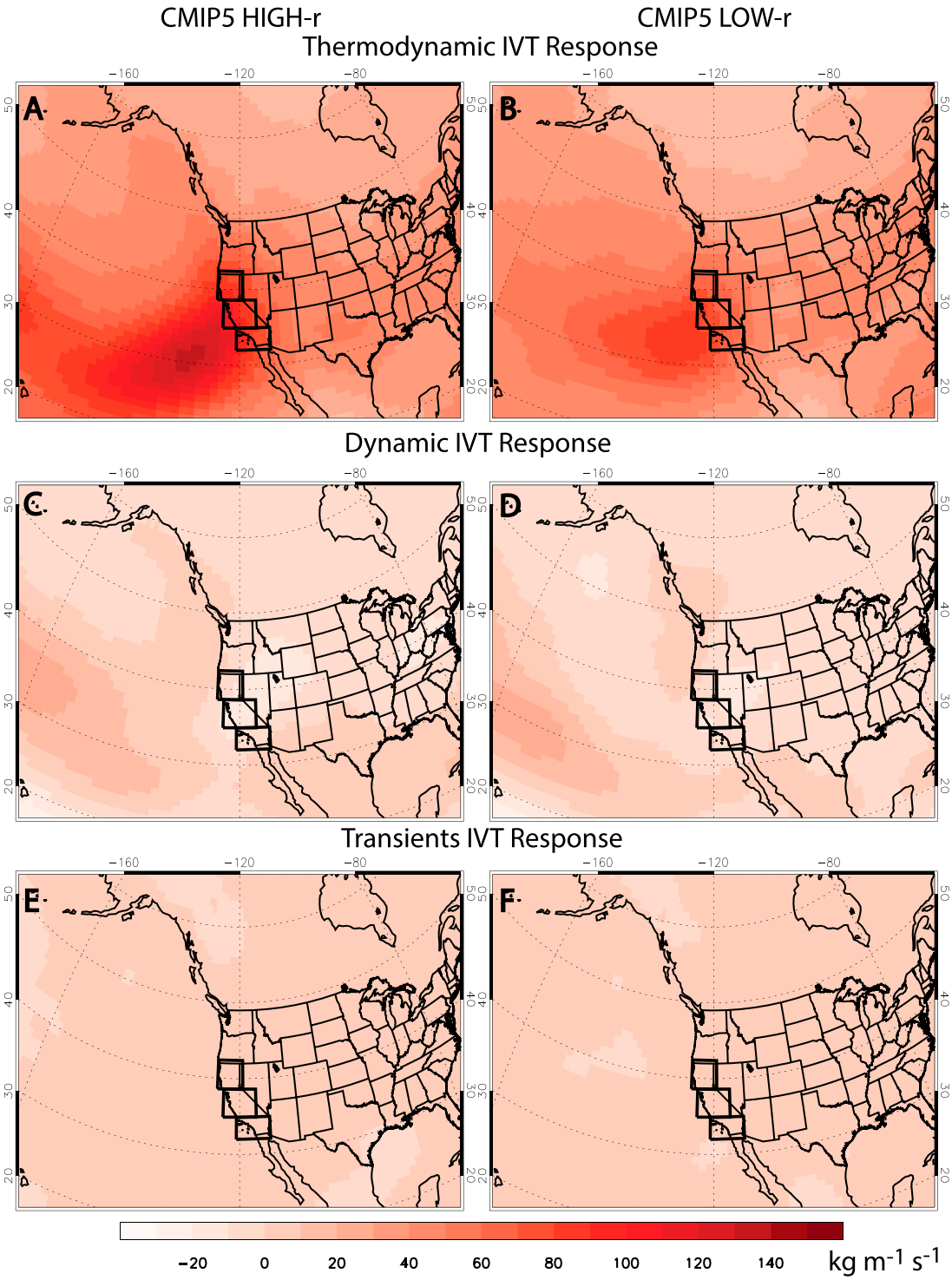

Figure 4. Integrated vapor transport component response associated with California wintertime extreme precipitation. Ensemble mean change (2050–2099 minus 1950–1999) in DJF IVT associated with extreme precipitation events due to (a, b) thermodynamic effects, (c, d) dynamic effects, and (e, f) transients. Left column shows the CMIP5 ensemble mean for the model subset that yields a detrended DJF Niño 3.4 sea surface temperature versus California precipitation correlation of at least 0.30 (HIGH−r); right column shows the model subset that yields a corresponding correlation less than 0.20 (LOW−r). Also included are the three regions comprising California. Units are kilograms per meter per second. DJF = December-January-February; IVT = integrated vapor transport; CMIP5 = Coupled Model Intercomparison Project version 5.

integrated vapor transport (IVT) off the CA coast (Figure 2). Although both model subsets also yield a similar relationship, CMIP5 LOW−r tends to underestimate this response. Most notably, the tongue of high PW and IVT that extends from the subtropics to CA is much weaker in CMIP5 LOW−r. The dynamical response associated with CA DJF extreme precipitation, which includes a low-pressure system off the CA coast and associated counterclockwise airflow, is also underestimated by CMIP5 LOW−r (supporting information Figures S5 and S6).

CMIP5 LOW−r underestimation of the tropical Pacific SST warming, and atmospheric response, on CA DJF extreme precipitation days is consistent with a corresponding underestimation of observed CA DJF extreme precipitation percentiles. Climate Prediction Center precipitation observations from 1950 to 1999 yield CA DJF extreme precipitation thresholds of 15.5, 19.5, and 29.7 mm/day for the 90th, 95th, and 99th percentiles. CMIP5 LOW−r yields corresponding percentiles of 13.4, 16.8, and 23.5 mm/day, whereas CMIP5 HIGH−r yields larger values at 15.8, 19.9 and 28.6 mm/day, respectively, and in better agreement to the observed percentiles (supporting information Figure S7). We note, however, that these differences are relatively small. Moreover, both model subsets tend to simulate similar total, nonextreme, and extreme DJF precipitation climatologies for CA and each of the three CA subregions (supporting information Figure S8). Both model subsets, as well as the entire CMIP5 ensemble, tend to overestimate DJF CA total precipitation, primarily due to overestimation of nonextreme precipitation, particularly in central CA.

Thus, simulation of CA DJF extreme precipitation is related to the ability of models to simulate the El Niño-CA precipitation teleconnection. CA DJF extreme precipitation is associated with anomalous warming of tropical Pacific SSTs. Models that underestimate this teleconnection also underestimate extreme precipitation percentiles—and the increase in PW and IVT—associated with CA DJF extreme precipitation.

Figure 3 shows the ensemble mean PW and IVT response (2050–2099 minus 1950–1999) associated with CA DJF extreme precipitation. Both model subsets yield an increase in IVT and PW in response to warming. However, CMIP5 HIGH−r models yield a larger increase in both, including a stronger tongue of high PW and IVT extending from the subtropics to CA. The dynamical response features a deeper and southeastward extended Aleutian low-pressure system and enhanced counterclockwise flow (supporting information Figure S9). However, this dynamical response is located quite far from the CA coast, with the bulk of the response in the Gulf of Alaska (and to the northwest of the low-pressure system associated with CA DJF extreme precipitation during the late twentieth century; supporting information Figure S5). Thus, this seems to suggest that the larger increase in CA DJF extreme precipitation in CMIP5 HIGH−r is due to thermodynamic effects.

Figure 4 confirms this notion and shows that the bulk of the increase in IVT associated with extreme precipitation is related to thermodynamic effects, as opposed to dynamic effects or transients (section 2). This result implies that the increase in atmospheric moisture, and not the change in winds, is the dominant cause of the 21st century IVT increase associated with CA DJF extreme precipitation. Furthermore, CMIP5 HIGH−r yields a larger increase in the thermodynamic IVT component associated with extreme precipitation, consistent with this model subset's larger increase in IVT, and extreme precipitation. The importance of thermodynamic effects is generally consistent with Payne and Magnusdottir (2015), although they note the possible importance of dynamical effects on the equatorward flank of the climatological IVT distribution.

4. Conclusions

In response to continued greenhouse gas emissions, CMIP5 models tend to project an increase in CA DJF precipitation, and nearly all of this increase is due to an increase in extreme (>90th percentile) daily precipitation. This is consistent with an increase in PW and integrated vapor transport off the CA coast during extreme precipitation events. Decomposition of the IVT response shows that the increase in atmospheric moisture dominates the increase in IVT associated with CA DJF extreme precipitation under warming.

Late twentieth century observations show that CA DJF extreme precipitation is associated with anomalous warming of the tropical Pacific, in addition to a low-pressure system and enhanced counterclockwise flow, as well as enhanced PW and IVT, off the CA coast. Models that better simulate the observed El Niño-CA DJF precipitation teleconnection (i.e., CMIP5 HIGH−r) also better simulate the thermodynamic and dynamic atmospheric responses associated with CA DJF extreme precipitation, as well as the corresponding extreme precipitation thresholds. Under warming, CMIP5 HIGH−r also yields significantly larger increases in CA DJF extreme precipitation relative to CMIP5 LOW−r, with more than double the increase. This is consistent with

a larger increase in PW and IVT in CMIP5 HIGH−r, which is again primarily due to an increase in atmospheric moisture associated with CA DJF extreme precipitation.

Since dynamical effects appear to be less important, the larger response in CMIP5 HIGH−r is related to its ability to better simulate the thermodynamical response associated with CA DJF extreme precipitation. Furthermore, both model subsets yield similar DJF climatological SST responses (supporting information Figure S10), which suggests that enhanced seasonal warming in CMIP5 HIGH−r (and the expected enhanced atmospheric moisture) is not the cause of the larger CMIP5 HIGH−r response. Our results therefore show the importance of model simulation of the El Niño teleconnection, particularly in the context of thermodynamical effects, to future enhancement of CA DJF extreme precipitation.

Acknowledgments
This study was funded by NSF award AGS-1455682. The authors declare that they have no competing financial interests. CMIP5 data can be downloaded from the data access portal at https://cmip.llnl.gov/cmip5/data_portal.html. NCEP/NCAR data can be downloaded from the Earth System Research Laboratory at https://www.esrl.noaa.gov/psd/data/gridded/data.ncep.reanalysis.html. CPC precipitation observations can also be obtained from the Earth System Research Laboratory at https://www.esrl.noaa.gov/psd/data/gridded/data.unified.daily.conus.html. NOAA AVHRR SST data can be obtained from NOAA at https://www.ncdc.noaa.gov/oisst.

References

Allen, R. J., & Luptowitz, R. (2017). *El Niño-like teleconnection increases California precipitation in response to warming*, vol. 8, pp. 16055. https://doi.org/10.1038/ncomms16055

Banzon, V., Smith, T. M., Chin, T. M., Liu, C., & Hankins, W. (2016). A long-term record of blended satellite and in situ sea-surface temperature for climate monitoring, modeling and environmental studies. *Earth System Science Data*, *8*(1), 165–176. https://doi.org/10.5194/essd–8–165–2016

Chang, E. K. M., Zheng, C., Lanigan, P., Yau, A. M. W., & Neelin, J. D. (2015). Significant modulation of variability and projected change in California winter precipitation by extratropical cyclone activity. *Geophysical Research Letters*, *42*, 5983–5991. https://doi.org/10.1002/2015GL064424

Chen, M., Shi, W., Xie, P., Silva, V. B. S., Kousky, V. E., Higgins, R. W., & Janowiak, J. E. (2008). Assessing objective techniques for gauge-based analyses of global daily precipitation. *Journal of Geophysical Research*, *113*, D04110. https://doi.org/10.1029/2007JD009132

Coats, S., Smerdon, J. E., Cook, B. I., & Seager, R. (2013). Stationarity of the tropical Pacific teleconnection to North America in CMIP5/PMIP3 model simulations. *Geophysical Research Letters*, *40*, 4927–4932. https://doi.org/10.1002/GRL50938

Deser, C., Simpson, I. R., McKinnon, K. A., & Phillips, A. S. (2017). The Northern Hemisphere extratropical atmospheric circulation response to ENSO: How well do we know it and how do we evaluate models accordingly. *Journal of Climate*, *30*, 5059–5082. https://doi.org/10.1175/JCLI–D–16–0844.1

Dettinger, M. D. (2011). Climate change, atmospheric rivers and floods in California—A multimodel analysis of storm frequency and magnitude changes. *Journal of American Water Resources Association*, *47*, 514–523. https://doi.org/10.1111/j.1752-1688.2011.00546.x

Hagos, S. M., Leung, L. R., Yoon, J.-H., Lu, J., & Gao, Y. (2016). A projection of changes in landfalling atmospheric river frequency and extreme precipitation over western North America from the Large Ensemble CESM simulations. *Geophysical Research Letters*, *43*, 1357–1363. https://doi.org/10.1002/2015GL067392

Kalnay, E., Kanamitsu, M., Kistler, R., Collins, W., Deaven, D., Gandin, L., et al. (1996). The NCEP/NCAR 40-year reanalysis project. *Bulletin of the American Meteorological Society*, *77*, 437–471.

Lavers, D. A., Ralph, F. M., Waliser, D. E., Gershunov, A., & Dettinger, M. D. (2015). Climate change intensification of horizontal water vapor transport in CMIP5. *Geophysical Research Letters*, *42*, 5617–5625. https://doi.org/10.1002/2015GL064672

Mamalakis, A., Yu, J.-Y., Randerson, J. T., AghaKouchak, A., & Foufoula-Georgiou, E. (2018). A new interhemispheric teleconnection increases predictability of winter precipitation in southwestern US. *Nature Communications*, *9*(1), 2332. https://doi.org/10.1038/s41,467–018–04722–7

Neelin, J. D., Langenbrunner, B., Meyerson, J. E., Hall, A., & Berg, N. (2013). California winter precipitation change under global warming in the Coupled Model Intercomparison Project Phase 5 ensemble. *Journal Climate*, *26*, 6238–6256. https://doi.org/10.1175/JCLI–D–12–00514.1

Pavia, E. G. (2017). Changes in the ENSO–rainfall relationship in the Mediterranean California border region. *Atmospheric Science Letters*, *18*, 183–186. https://doi.org/10.1002/asl.741

Payne, A. E., & Magnusdottir, G. (2015). An evaluation of atmospheric rivers over the North Pacific in CMIP5 and their response to warming under RCP8.5. *Journal of Geophysical Research: Atmospheres*, *120*, 11,173–11,190. https://doi.org/10.1002/2015JD023586

Polade, S. D., Gershunov, A., Cayan, D. R., Dettinger, M. D., & Pierce, D. W. (2017). Precipitation in a warming world: Assessing projected hydro-climate changes in California and other Mediterranean climate regions. *Scientific Reports*, *7*(1), 10,783. https://doi.org/10.1038/s41,598–017–11285–y

Reynolds, R. W., Smith, T. M., Liu, C., Chelton, D. B., Casey, K. S., & Schlax, M. G. (2007). Daily high-resolution-blended analyses for sea surface temperature. *Journal of Climate*, *20*(22), 5473–5496. https://doi.org/10.1175/2007JCLI1824.1

Seager, R., Naik, N., & Vecchi, G. A. (2010). Thermodynamic and dynamic mechanisms for large-scale changes in the hydrological cycle in response to global warming. *Journal of Climate*, *23*, 4651–4668. https://doi.org/10.1175/2010JCLI3655.1

Seager, R., Neelin, D., Simpson, I., Liu, H., Henderson, N., Shaw, T., et al. (2014). Dynamical and thermodynamical causes of large-scale changes in the hydrological cycle over North America in response to global warming. *Journal Climate*, *27*, 7921–7948. https://doi.org/10.1175/JCLI–D–14–00153.1

Swain, D. L., Langenbrunner, B., Neelin, J. D., & Hall, A. (2018). Increasing precipitation volatility in twenty-first-century California. *Nature Climate Change*, *8*(6), 427–433. https://doi.org/10.1038/s41,558–018–0140–y

Taylor, K. E., Stouffer, R. J., & Meehl, G. A. (2012). An overview of CMIP5 and the experiment design. *Bulletin of the American Meteorological Society*, *93*, 485–498.

Trenberth, K. E., & Guillemot, C. J. (1995). Evaluation of the global atmospheric moisture budget as seen from analyses. *Journal Climate*, *8*, 2255–2272. https://doi.org/10.1175/1520–0442(1995)008<2255:EOTGAM>2.0.CO;2

Warner, M. D., Mass, C. F., & Salathé, E. P. (2015). Changes in winter atmospheric rivers along the North American West Coast in CMIP5 climate models. *Journal of Hydrometeorology*, *16*(1), 118–128. https://doi.org/10.1175/JHM–D–14–0080.1

Wehner, M. F., Smith, R. L., Bala, G., & Duffy, P. (2010). The effect of horizontal resolution on simulation of very extreme US precipitation events in a global atmosphere model. *Climate Dynamics*, *34*(2), 241–247. https://doi.org/10.1007/s00382–009–0656–y

Xie, P., Yatagai, A., Chen, M., Hayasaka, T., Fukushima, Y., Liu, C., & Yang, S. (2007). A gauge-based analysis of daily precipitation over East Asia. *Journal of Hydrometeorology*, *8*, 607–626.